Rheol. Acta **16**, 291–301 (1977)

ISSN 0035-4511/ASTM-Coden: RHEAAK

Chemical Engineering and Materials Science and Engineering Departments, Northwestern University, Evanston, Illinois (USA)

Experimental tests of constitutive relations for polymers undergoing uniaxial shear flows

W. W. Graessley, W. S. Park, and *R. L. Crawley*

With 15 figures and 1 table

(Received December 15, 1976)

1. Introduction

One of the aims in polymer rheology is to discover simple constitutive relationships which, from the results of a limited set of experiments, can be used to calculate stress with tolerable accuracy for a wide variety of deformation histories. Methods for measuring linear viscoelastic properties and steady state stress in steady uniaxial shear flows are fairly well established (1, 2). Certain asymptotic relationships between material functions for these two classes are expected on rather general grounds (3) and have been confirmed (see ref. 4, for example). Several constitutive equations, though based on different hypotheses, appear to be more or less equivalent in their ability to fit experimental behavior in both classes. However, their predictions differ markedly for other flow histories. Recently it has become possible to test some of these hypotheses directly, using data on the growth of stress to steady state after the sudden start-up of steady uniaxial shear flow and the relaxation of stress from steady state after its sudden cessation. The purpose of this paper is to describe such tests with data obtained with a specially stiffened Weissenberg Rheogoniometer. Three solutions of polystyrene were used, ranging in zero shear viscosity from 890 poise to 67,000 poise.

The steady state components of shear stress σ and first normal stress difference N_1 in steady shear flow are related to shear rate $\dot{\gamma}$ by

$$\sigma(\dot{\gamma}) = \eta(\dot{\gamma})\,\dot{\gamma}\,, \qquad [1]$$

$$N_1(\dot{\gamma}) = \Psi(\dot{\gamma})\,\dot{\gamma}^2\,, \qquad [2]$$

in which $\eta(\dot{\gamma})$ is the viscosity of the material and $\Psi(\dot{\gamma})$ is the first normal stress coefficient. Both η and Ψ are positive for all $\dot{\gamma}$ and approach constant values, η_0 and Ψ_0, at sufficiently small shear rates. The time and shear rate dependence of the stress components following start-up ($\dot{\gamma} = 0$ for $t < 0$; $\dot{\gamma} =$ constant for $t > 0$) will be indicated by $\hat{\sigma}(\dot{\gamma}, t)$ and $\hat{N}_1(\dot{\gamma}, t)$, while those following cessation ($\dot{\gamma} =$ constant for $t < 0$, $\dot{\gamma} = 0$ for $t > 0$) will be indicated by $\check{\sigma}(\dot{\gamma}, t)$ and $\check{N}_1(\dot{\gamma}, t)$. Clearly,

$$\hat{\sigma}(\dot{\gamma}, \infty) = \check{\sigma}(\dot{\gamma}, 0) = \eta(\dot{\gamma})\,\dot{\gamma}\,, \qquad [3]$$

$$\hat{N}_1(\dot{\gamma}, \infty) = \check{N}_1(\dot{\gamma}, 0) = \Psi(\dot{\gamma})\,\dot{\gamma}^2\,, \qquad [4]$$

$$\hat{\sigma}(\dot{\gamma}, 0) = \check{\sigma}(\dot{\gamma}, \infty) = \hat{N}_1(\dot{\gamma}, 0) = \hat{N}_1(\dot{\gamma}, \infty) = 0\,. \qquad [5]$$

Linear viscoelastic properties are governed by the relaxation time distribution or relaxation spectrum $H(\tau)$. In uniaxial shear flows the shear stress from sufficiently slow or sufficiently small deformations is given by (5)

$$\sigma(t) = \int_{-\infty}^{t} m(t - t')\,[\gamma(t) - \gamma(t')]\,dt' \qquad [6]$$

in which $\gamma(t)$ is the shear deformation at time t measured from some arbitary reference shape and

$$m(\xi) = -\frac{dG}{d\xi} = \int_{-\infty}^{\infty} \frac{H(\tau)}{\tau} e^{-\frac{\xi}{\tau}}\,d\ln\tau \qquad [7]$$

in which $G(\xi)$ is the shear stress relaxation modulus. In the same limit, the first normal stress difference also depends on $m(\xi)$ alone and hence $H(\tau)$ (5):

$$N_1(t) = \int_{-\infty}^{t} m(t - t')\,[\gamma(t) - \gamma(t')]^2\,dt'\,. \qquad [8]$$

The following relationships connect the steady state and linear viscoelastic functions (3)

$$\eta_0 = \int_{-\infty}^{\infty} \tau H(\tau)\, d\ln\tau = \lim_{\dot\gamma\to 0} \eta(\dot\gamma), \qquad [9]$$

$$J_e^0 = \frac{\int_{\infty}^{\infty} \tau^2 H(\tau)\, d\ln\tau}{\left[\int_{-\infty}^{\infty} \tau H(\tau)\, d\ln\tau\right]^2} = \frac{1}{2\eta_0^2} \lim_{\dot\gamma\to 0} \psi(\dot\gamma), \qquad [10]$$

in which η_0 is the zero shear viscosity and J_e^0 is the steady state recoverable shear compliance. Likewise, for $\dot\gamma$ sufficiently small the shear and normal stress during start-up and relaxation from steady state depend on $H(\tau)$ through the following monotonic functions of $\dot\gamma$ and t (from eqs. [6]–[8]):

$$\hat\sigma(\dot\gamma, t) = \dot\gamma \int_{-\infty}^{\infty} \tau H(\tau)\left[1 - e^{-t/\tau}\right] d\ln\tau, \qquad [11]$$

$$\hat N_1(\dot\gamma, t) = 2\dot\gamma^2 \int_{-\infty}^{\infty} \tau^2 H(\tau)\left[1 - (1+\tfrac{t}{\tau})e^{-t/\tau}\right] d\ln\tau, \qquad [12]$$

$$\check\sigma(\dot\gamma, t) = \dot\gamma \int_{-\infty}^{\infty} \tau H(\tau)\, e^{-t/\tau}\, d\ln\tau, \qquad [13]$$

$$\check N_1(\dot\gamma, t) = 2\dot\gamma^2 \int_{-\infty}^{\infty} \tau^2 H(\tau)\, e^{-t/\tau}\, d\ln\tau. \qquad [14]$$

These limiting forms should be applicable to a very broad class of viscoelastic fluids for all times at sufficiently small $\dot\gamma$ and, in the case of eqs. [11] and [12], for sufficiently short times at any $\dot\gamma$.

We will restrict the discussion to single integral constitutive equations, of which the Lodge eq. [6] is a basic form:

$$\boldsymbol{p}(t) = \int_{-\infty}^{t} M(t-t')\boldsymbol{C}^{-1}(t,t')\, dt' - P_0\boldsymbol{I}. \qquad [15]$$

Here $\boldsymbol{p}(t)$ is the total stress at time t, $\boldsymbol{C}^{-1}(t', t)$ the Finger strain tensor, $M(t-t')$ the memory function of the fluid, P_0 an arbitrary pressure and $\boldsymbol{I}$ the unit tensor. The stress at current time t is thus the sum of contributions from strains at all past times t' relative to the current configuration, each weighted by a function which depends only on the elapsed time $t-t'$. The Lodge equation reduces directly to eqs. [14]–[16] for start-up and relaxation at all shear rates.

Other single integral equations involve flow related modifications of the memory function. In one group the contributions of past strains depend on the strain rate (7) or the relative strain (8) at t'. For σ und N_1 in uniaxial shear flows the memory function in eq. [15] can be expressed as

$M(|\dot\gamma(t')|,\ t-t')$ (strain rate models)

and

$M(\gamma(t)-\gamma(t'),\ t-t')$ (relative strain models).

Note that the memory function in such cases depends on the state of the system at no other times than t and t'.

In another group of equations the memory function depends on the motion at all intervening times between t and t' (9, 10). For σ and N_1 in uniaxial shear flows these memory functions can be expressed as

$M(|\bar{\dot\gamma}(t')|,\ \bar{\dot\gamma}(t', t),\ t-t')$ (averaged rate models),

in which $\bar{\dot\gamma}(t', t)$ is an average shear rate over the interval between t' and t. The method of averaging varies from one formulation to another.

Marrucci and coworkers (11) have recently proposed an equation in which the memory function depends on a structural parameter whose values are in turn a function of the entire history of the motion. That is, the contribution of strain at past time t' depends not just on elapsed time $t-t'$ and events between t' and t but also on events prior to t'. The model is cast in a specific form such that the structural parameter depends on both the past motion and past values of the stress. In a rough way we can express this memory function for uniaxial shear flows as

$M(x(t', t),\ t-t')$ (structural model),

remembering that the structural parameter $x(t', t)$ is governed separately by the motion before t' as well. This list of memory function modifications is by no means exhaustive. Others have been proposed, such as those listed in table 6.4 (1) of reference (5).

Both the strain rate and relative strain models can be tested for consistency with start-up behavior without determining the memory function. *Van Es* and *Christensen* have shown that $\hat\sigma$ and $\hat N_1$ for fluids described by strain rate models must obey the following relation (12):

$$\int_{-\infty}^{\infty} \tau^2 H(\tau)\left[1 - (1+\tfrac{t}{\tau})\, e^{-t/\tau}\right] d\ln\tau = \frac{\hat N_1(\dot\gamma, t)}{\dot\gamma^2} - \frac{\Gamma(\dot\gamma, t)}{\dot\gamma} \qquad [16]$$

in which

$$\Gamma(\dot\gamma, t) = t\,\hat\sigma(\dot\gamma, t) - \int_0^t \hat\sigma(\dot\gamma, \lambda)\, d\lambda\,. \qquad [17]$$

The left side of eq. [16] is independent of shear rate and increases monotonically with time. The combination on the right side, involving the experimental start-up functions, must then behave likewise.

Yamamoto (7) has developed a second consistency relation for rate models governing stress during relaxation from steady state. In integral form (13):

$$\check N_1(\dot\gamma, t) = 2\dot\gamma \int_t^\infty \check\sigma(\dot\gamma, \lambda)\, d\lambda\,. \qquad [18]$$

Kearsley and *Zapas* (13, 14) have developed consistency tests for relative strain models. In this case the shear stress start-up curves can be used to predict normal stress start-up:

$$\hat N_1(\dot\gamma, t) = \dot\gamma\left[\Gamma(\dot\gamma, t) + \int_0^t \frac{\Gamma(\xi, t)}{\xi}\, d\xi\right] \qquad [19]$$

in which $\Gamma(\dot\gamma, t)$ is given by eq. [17]. Similarly, $\hat\sigma(\dot\gamma, t)$ can be predicted from $\hat N_1(\dot\gamma, t)$ data:

$$\hat\sigma(\dot\gamma, t) = \frac{1}{\dot\gamma}\left[\Lambda(\dot\gamma, t) - \int_0^t \frac{\Lambda(\xi, t)}{\xi}\, d\xi\right] \qquad [20]$$

in which

$$\Lambda(\dot\gamma, t) = \frac{\hat N_1(\dot\gamma, t)}{t} + \int_0^t \frac{\hat N_1(\dot\gamma, \lambda)}{\lambda^2}\, d\lambda\,. \qquad [21]$$

Note that in order to apply these relations it is necessary to integrate experimental data on $\hat\sigma$ and $\hat N_1$ from $\dot\gamma = 0$ to the shear rate of interest. It is therefore useful to have data extending to low enough shear rates that the limiting forms, given by eqs. [11] and [12], are reached. Extension to zero can then be accomplished by appropriate use of those functions.

Kearsley and *Zapas* have also developed a consistency relation for stress during relaxation from steady state in relative strain models:

$$\int_0^t \frac{\check N_1(\xi, t)}{\xi}\, d\xi = \dot\gamma \int_t^\infty \check\sigma(\dot\gamma, \lambda)\, d\lambda\,. \qquad [22]$$

There appears to be no consistency test available for the averaged rate and structural models in uniaxial shear flows, neither in general nor for the various special forms proposed. A form for the memory function must be selected; judgement of a model thus rests on its ability to fit the individual flow functions.

It seems to us that one should first insist that linear viscoelastic data be fitted well, since all models must reduce to linear viscoelastic behavior in the limit. Thus, $H(\tau)$ should be obtained as precisely as possible from linear viscoelastic data such as the dynamic moduli $G'(\omega)$ and $G''(\omega)$. The form of $H(\tau)$ should not be restricted by the form of the model. Acceptability of $H(\tau)$ should be judged not only by its ability to reproduce the $G'(\omega)$ and $G''(\omega)$ data but also by the agreement it produces between observed limiting start-up and relaxation functions and those calculated from eqs. [11]–[14]. With $H(\tau)$ determined, the steady state data, $\sigma(\dot\gamma)$ and $N_1(\dot\gamma)$, should be accommodated by adjustment of a relatively few model parameters, the effect of which should vanish for both sufficiently slow or sufficiently small deformations. In principle there should be no adjustable parameters, but considering the experimental uncertainties and the necessarily limited range which can be covered, it it quite possible that two polymers could appear to be identical in linear viscoelastic properties and yet show significantly different behavior in other types of flow. Once these adjustments have been made the ability of the model to predict start-up and relaxation from steady state should be judged without further changes.

2. Experimental

The start-up and relaxation of σ and N_1 were measured over wide ranges of shear rate and time for cone-plate flow in a modified Weissenberg Rheogoniometer (Model R 16). The axial force servo system was removed and the LVDT transducers replaced by piezoelectric crystals (15). These and other modifications, similar to those employed by *Meissner* (16), were made to increase axial and torsional stiffness and thereby diminish unwanted motion in the cone-plate assembly during transient stress measurements. The result was a total axial stiffness of approximately 2 kg/micron and total torsional stiffness of approximately 10^4 kg/-cm/rad (15).

Measurements were made at 25 °C on three solutions of polystyrene in tri-cresyl phosphate. The solution designated *A* is a 8% by weight solution of equal weights of two narrow distribution samples from Pressure Chemical Company (Pc 3a, $\bar M_w = 440{,}000$; Pc 14a, $\bar M_w = 1{,}800{,}000$) and has a zero shear viscosity of 890 poise at 25 °C. Solution B is an 8% by weight solution of Pc 14a alone and has a zero shear viscosity of 3900 poise. Solution *C* is 12% by weight of Pc 14a alone and has a zero shear viscosity of 67,000 poise.

The viscosity of tri-cresyl phosphate at 25°C is 0.70 poise.

Values of σ and N_1 were calculated during start-up, at steady state, and during relaxation from the torque and total axial force:

$$\sigma = \frac{3T}{2\pi R^3} \qquad [23]$$

$$N^1 = \frac{2F}{\pi R^2}, \qquad [24]$$

$$\dot{\gamma} = \frac{\Omega}{\tan\theta}, \qquad [25]$$

in which T is the torque, F is the axial force, Ω is the angular velocity, R is the platen radius, and θ is the gap angle. Data were collected with several gap angles ($\theta = 1°, 2°, 4°$, and 8°) and platen diameters ($D = 2R =$ 2.5 cm, 5.0 cm, and 7.5 cm). The steady state values of σ and N_1 obtained with the different angles and diameters agreed within 3% (15). The shear stress transients in start-up and relaxation were similarly insensitive to gap angle and platen diameter. The apparent normal stress transients varied with gap angle and, to a lesser extent, with platen diameter, as was noted by *Meissner* (16). The dependence diminished with increasing gap angle, such that data at 4° and 8° were in quite good agreement for the lower viscosity solutions *A* and *B*. Some small but systematic differences between 4° and 8° remained for solution *C*. The data discussed here were obtained with a 4° gap angle and the 2.5 cm and 7.5 cm platens for solutions *A* and *B*, and with an 8° gap angle and the 2.5 cm and 5.0 cm platens for solution *C*. Each transient is the average of two or three high speed recorder traces with the instrument run in both the forward and reverse directions. Further details are given elsewhere (15, 17).

The dynamic shear moduli $G'(\omega)$ and $G''(\omega)$ were measured for solutions *B* and *C* in the Rheometrics Mechanical Spectrometer (RMS) at 25°C. The eccentric parallel disc method was used, and corrections for instrument compliance were applied (18). Diameters of 2.5 cm (plate separation > 1.2 mm) and 7.2 cm (plate separation > 3 mm) were used for solution *C*. Owing to a shortage of sample, only the 2.5 cm diameter was used for solution *B*. Steady state values of σ and N_1 for solution *C* were also measured with the RMS using the cone-plate geometry (platen diameter 2.5 cm; gap angle 2.29°).

The values of $\eta(\dot{\gamma})$ and $N_1(\dot{\gamma})$ from the two instruments agreed fairly well over their common range, but it was not possible to reach the η_0 limit with the Mechanical Spectrometer for solution *C*. The values of $\eta'(\omega)$ at low frequencies leveled off at 67,000 poise, somewhat larger than the value, $\eta_0 = 58{,}000$ poise, reported from Rheogoniometer data (15). We believe the apparent difference in η_0 is related to the rather long time required to reach steady state at low shear rates in solution *C*. Behavior at long times and low stresses is particularly difficult to measure in the modified Rheogoniometer due to drift in the piezoelectric signal baseline. The value of 67,000 poise from $\eta'(\omega)$ in the Mechanical Spectrometer is believed to be correct for solution *C*.

The dynamic and steady state data for solutions *B* and *C* are plotted in figures 1 and 2. Steady state data obtained on the Rheogoniometer alone for all three solutions are given elsewhere (15).

The relaxation spectrum $H(\tau)$ was obtained from $G''(\omega)$ as follows. An initial estimate was made with *Tschoegl*'s second approximation formula (1):

$$H_0(\tau) = \frac{2}{\pi}\left[G''(\omega) - \frac{4}{3}\frac{dG''}{d\ln\omega} + \frac{1}{3}\frac{d^2G''}{d(\ln\omega)^2}\right]_{\omega = 5^{1/2}/\tau}. \qquad [26]$$

Values of $G''(\omega)$ were then calculated from $H_0(\tau)$ for comparison with the observed $G''(\omega)$:

$$G''(\omega) = \int_{-\infty}^{\infty} H_0(\tau)\frac{\omega\tau}{1+\omega^2\tau^2}\, d\ln\tau. \qquad [27]$$

The departures were then used to refine the spectrum:

$$H_1(\tau) = H_0(\tau)[[G''(\omega)]_{\text{obs.}}/[G''(\omega)]_{\text{calc.}}]_{\omega = 1/\tau}. \qquad [28]$$

This procedure was repeated until the refined spectrum no longer changed significantly. The magnitude of $H(\tau)$ at long times was still incorrect however, as judged by values of η_0 and J_e^0 calculated from $H(\tau)$ with eqs. [9] and [10] and those obtained directly

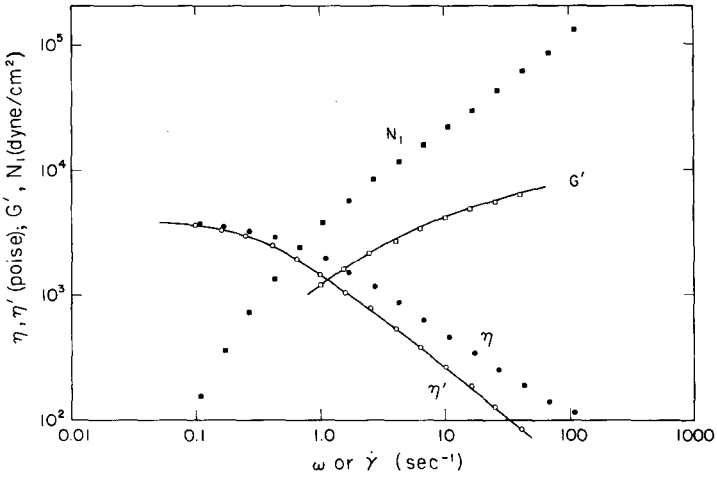

Fig. 1. Steady state and dynamic data for solution *B*. The solid lines are G' and $\eta'(G''/\omega)$ calculated from the relaxation spectrum of solution *B* (fig. 3)

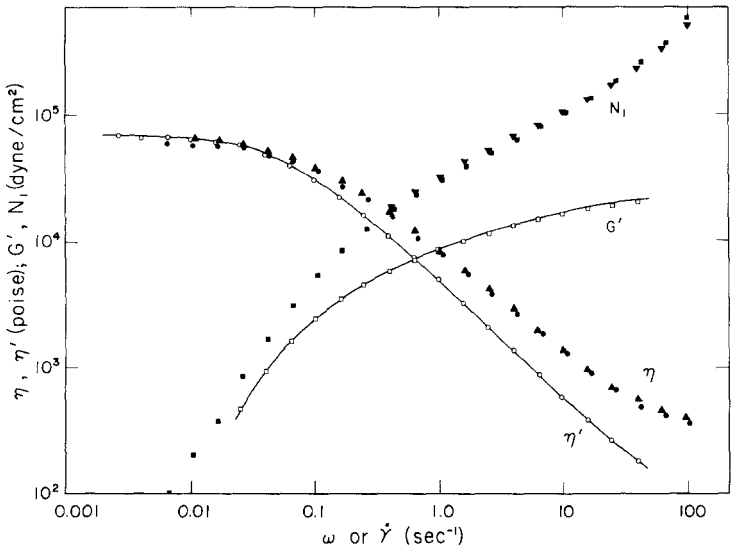

Fig. 2. Steady state and dynamic data for solution C. The solid lines are G' and η' calculated from the relaxation spectrum of solution C (fig. 3). Steady state data were obtained on both the rheogoniometer (●, ■) and the mechanical spectrometer (▲, ▼)

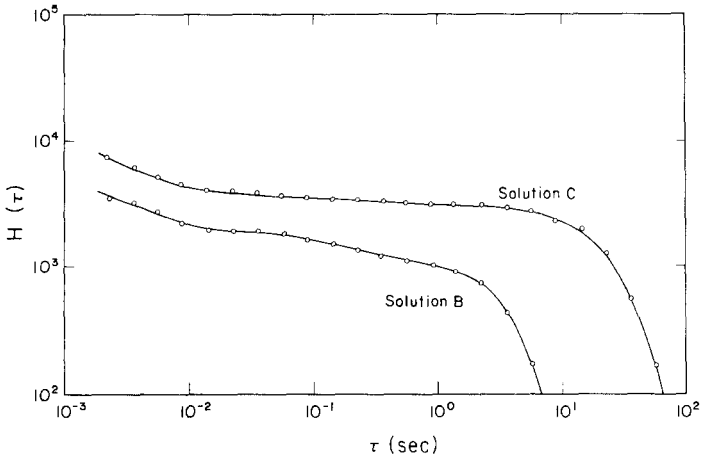

Fig. 3. Relaxation spectra calculated from $G''(\omega)$ for solutions B and C

from the experimental data. The spectrum was then modified by successively removing the long time relaxations until agreement with η_0 and J_e^0 was obtained The final spectra for solutions B and C are shown in figure 3. Comparisons of η_0 and J_e^0 are given in table 1. The solid lines drawn through the $\eta'(\omega)$ and $G'(\omega)$ data in figures 1 and 2 were calculated from these spectra.

Table 1. Comparison of viscoelastic parameters obtained by different. Instruments and methods for solutions B and C

	Solution B (8%)	Solution C (12%)
η_0(WRG, η)	3.9×10^3 poise	5.9×10^4 poise
η_0(RMS, η)	–	6.7
η_0(RMS, η')	3.9	6.7
$\eta_0(H(\tau))$	3.99	6.95
J_e^0(WRG, $N_1/2\sigma^2$)	4.3×10^{-4} cm²/dyne	2.0×10^{-4} cm²/dyne
J_e^0(RMS, G'/G''^2)	4.5	2.1
$J_e^0(H(\tau))$	6.08	2.46

WRG = Weissenberg Rheogoniometer
RMS = Rheometrics Mechanical Spectrometer

3. Results

The start-up curves for shear stress and normal stress in solution B ($\dot\gamma \geq 0.107$ sec^{-1}) are shown in figures 4 and 5. Data were obtained at every other gearbox setting, so the shear rates are equally spaced on a logarithmic scale: $\dot\gamma_i = 1.585\,\dot\gamma_{i-1}$. For legibility only curves at every other shear rate are plotted. The data are plotted as $\hat\sigma(\dot\gamma, t)/\dot\gamma$ and $\hat N_1(\dot\gamma, t)/\dot\gamma^2$ vs. t such that the limiting behavior at low shear rates should lie along a single curve (19, 20). In each case the curves appear to lie within a limiting envelope. The dashed lines are the limiting curves calculated from $H(\tau)$ using eqs. [11] and [12]. Agreement with the limiting envelope appears to be fairly good for $\hat\sigma$. Agreement is also good for $\hat N_1$ except at long times where the experimental

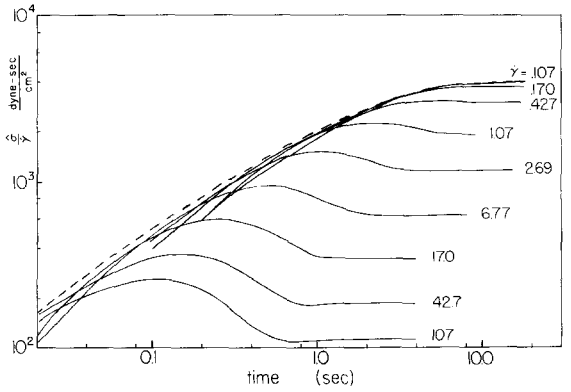

Fig. 4. Start-up curves for shear stress in solution *B*. The dashed line is the limiting start-up curve calculated from $H(\tau)$ using eq. [11]

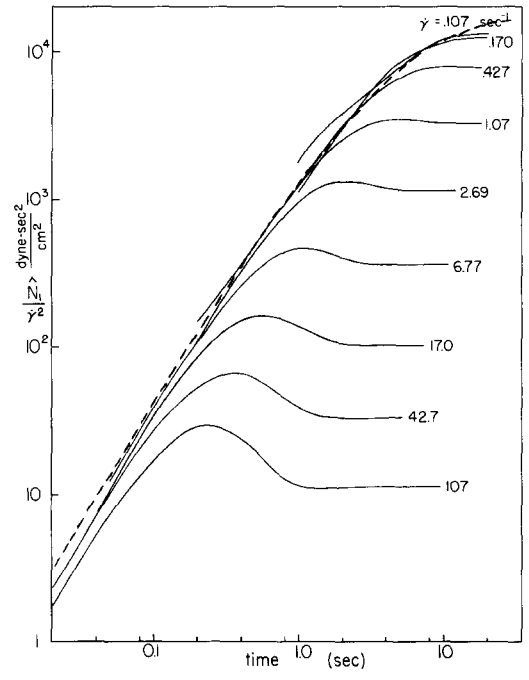

Fig. 5. Start-up curves for normal stress in solution *B*. The dashed line is the limiting start-up curve calculated from $H(\tau)$ using eq. [12]

values fall below the calculated curve. This could be caused by small errors in the long-time end of the spectrum or, more likely, by difficulties in measuring small values of N_1 at long times, owing to baseline drift. Similar data were obtained with solution *C* for $\dot{\gamma} \geq 0.0427$ sec^{-1}. In solution *C* neither $\hat{\sigma}$ nor $\hat{N}_1$ data reached the limiting curves at long times.

The start-up data appear to follow the limiting curves for some period of time. They then depart at times which decrease with increasing shear

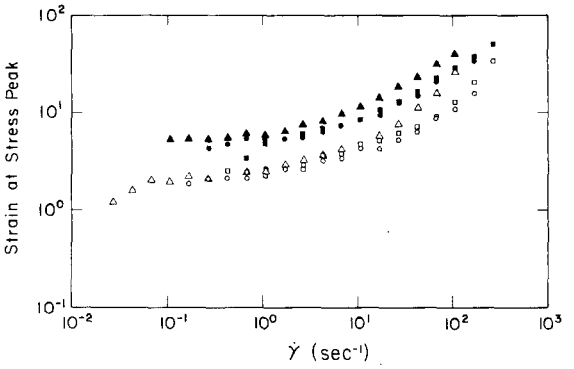

Fig. 6. Strain at the stress peaks in the start-up curves. The open symbols indicate shear stress peaks in solution *A* (□), solution *B* (○) and solution *C* (△); the filled symbols indicate normal stress peaks in solution *A* (■), solution *B* (●) and solution *C* (▲)

rate, pass through increasing prominent maxima, and finally approach steady state values of $\eta(\dot{\gamma})$ and $\psi(\dot{\gamma})$. The positions of the maxima correlate most directly with total strain, as many workers have noted previously. Figure 6 shows strain at the stress peak as a function of shear rate. At low shear rates the $\hat{\sigma}$ and $\hat{N}_1$ strains at peak tend to constant values which are practically the same for all three solutions. They then increase slowly with shear rate. The ratio of peak strains (or ratio of times to peak) for $\hat{\sigma}$ and $\hat{N}_1$ is shown in figure 7 as a function

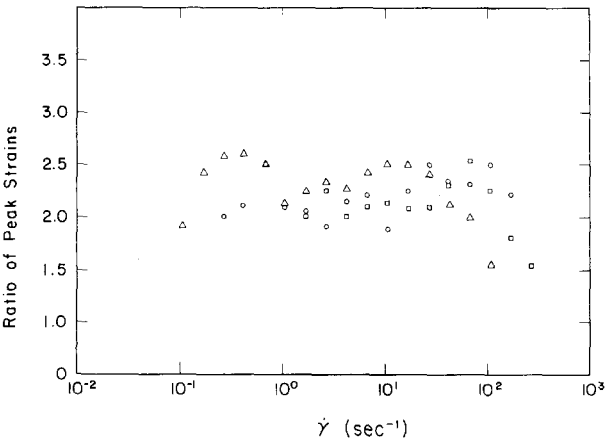

Fig. 7. Ratio of strain at normal stress peak to strain at shear stress peak in the start-up curves. The symbols indicate solution *A* (□), solution *B* (○) and Solution *C* (△)

of shear rate. The peak strain ratio is similar for all three solutions, being approximately 2.3. There is no observable trend with shear rate.

4. Strain rate models

The two criteria of *Van Es* and *Christensen* for strain rate models were examined with start-up data from all three solutions. Neither was satisfied except at the limit of low shear rates. The right side of eq. [16], calculated from experimental data, was not independent of shear rate. It was also not always monotonic in time, since at high shear rates the curves passed through shallow but definite maxima. Figure 8 shows the behavior at selected shear rates for solution *B*. Others have noted similar failures for strain rate models (12, 21). Interestingly, the relaxation criterion for rate models appears to be satisfied, at least judged by the values of $N_1(\dot{\gamma})$, calculated from eq. [18] for $t = 0$:

$$N_1(\dot{\gamma}) = 2\dot{\gamma} \int_0^\infty \check{\sigma}(\dot{\gamma}, \lambda)\, d\lambda \,. \qquad [29]$$

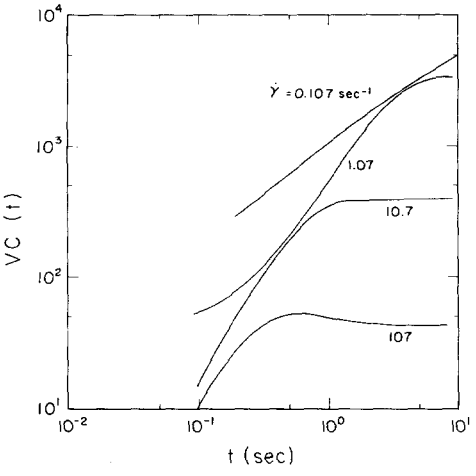

Fig. 8. van Es-Christensen function at various shear rates for solution *B*. The ordinate $VC(t)$ is the right side of eq. [16] in units of dyne-sec^2/cm^2

For example, the calculated value of N_1 is 4800 dyne/cm^2 at $\dot{\gamma} = 1.07\,\text{sec}^{-1}$ and 22000 dyne/cm^2 at $\dot{\gamma} = 10.7\,\text{sec}^{-1}$ for solution *B*, while values of 3800 and 22000 dyne/cm^2 are observed experimentally. However, in view of the rate model failure in start-up we did not test the relaxation behavior in any detail.

5. Relative strain models

Consistency of start-up stress with relative strain models was examined using eqs. [19] and [20]. The numerical integrations over shear rate at constant time need careful handling, as pointed out by *Kearsley* and *Zapas* (14). Fortunately, data to define the limiting behavior (eqs. [11] and [12]) for solutions *B* and *C* were available, so the integrals could be extended down to $\dot{\gamma} = 0$ quite easily. Figures 9, 10 and 11 show the tests with start-up data for solution *B* at three shear rates.

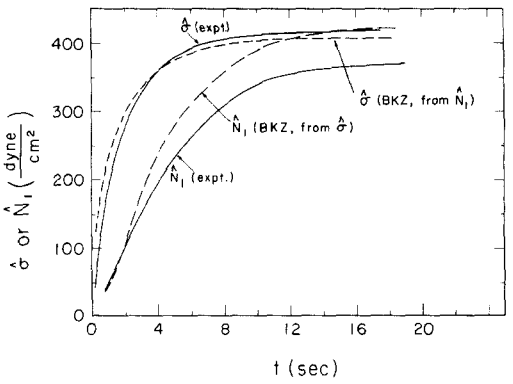

Fig. 9. Comparison of calculated and observed start-up curves for solution *B* at $\dot{\gamma} = 0.107\,\text{sec}^{-1}$. The dashed curves are calculated using the *Kearsley* consistency relations for relative strain models (eqs. [19] and [20])

In Figure 9 the shear rate is very near the limiting region, there is no overshoot in $\hat{\sigma}$ and $\hat{N}_1$, and the agreement between observed and calculated values is acceptable. The experimental $\hat{\sigma}$ curve is close to that calculated from $\hat{N}_1$, and if the $\hat{N}_1$ curve calculated from $\hat{\sigma}$ were scaled to give the same steady state value as the experimental $\hat{N}_1$ (an adjustment of about 12%), those two curves would practically coincide. On the other hand, since the data lie very near the limiting curve, such agreement constitutes not so much a test of relative strain models as a confirmation that such models reduce to the correct limiting forms at sufficiently low shear rates.

In figure 10 the shear rate lies just beyond the knee of the viscosity curve; in figure 11 it is well into the power law region. Systematic differences now appear between the observed and calculated values of $\hat{N}_1$. In figure 11 the calculated values of $\hat{N}_1$ actually become negative. Interestingly, the observed $\hat{\sigma}$ and values calculated from the $\hat{N}_1$ data do not show such extreme discrepancies. In both $\hat{\sigma}$ and $\hat{N}_1$ the agreement with calculated values at short times (before the maxima) is fairly good. Similar results are found at other shear rates and for solutions *A* and *C* as well.

Figures 12 and 13 show the consistency tests for relaxation behavior in solution *B* at the

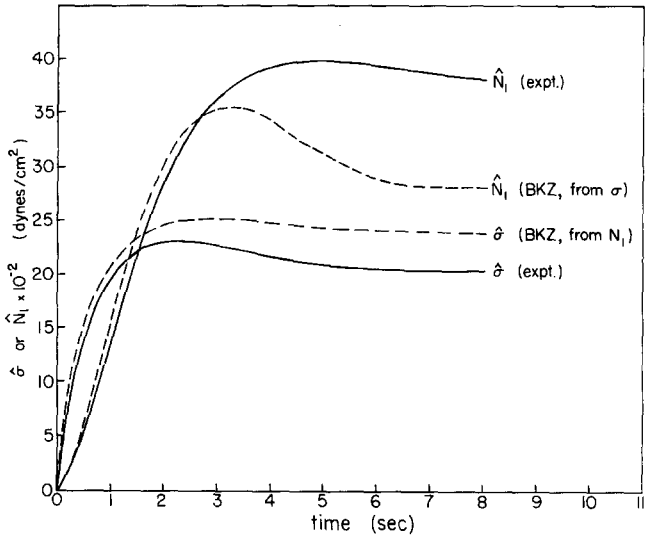

Fig. 10. Comparison of calculated and observed start-up curves for solution *B* at $\dot{\gamma} = 1.07\ \text{sec}^{-1}$ (see fig. 9 caption)

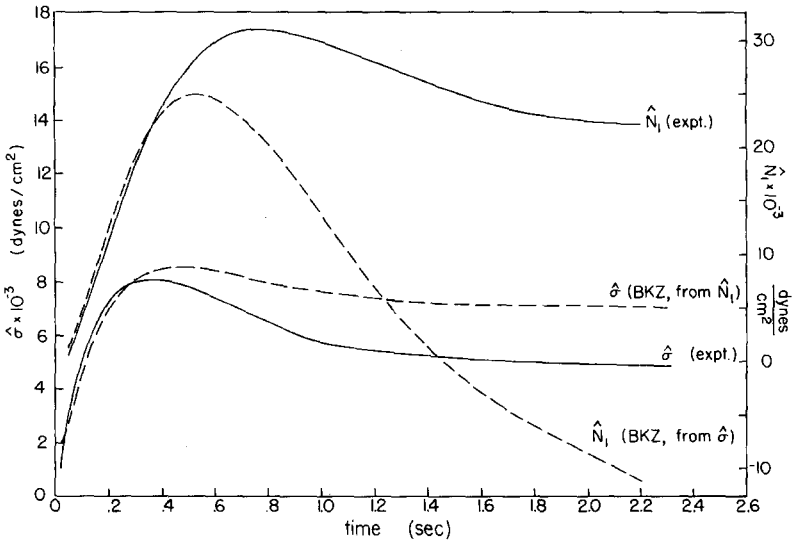

Fig. 11. Comparison of calculated and observed start-up curves for solution *B* at $\dot{\gamma} = 10.7\ \text{sec}^{-1}$ (see fig. 9 caption)

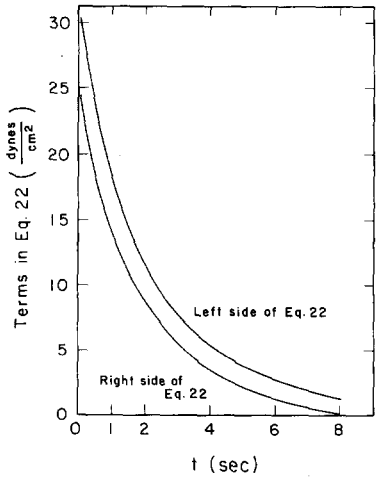

Fig. 12. Consistency test for relative strain models with relaxation data on solution *B* for $\dot{\gamma} = 1.07\ \text{sec}^{-1}$

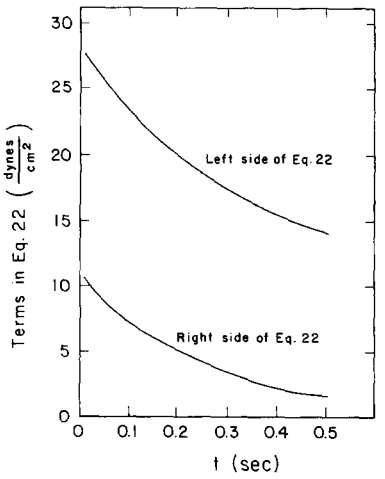

Fig. 13. Consistency test for relative strain models with relaxation data on solution *B* for $\dot{\gamma} = 10.7\ \text{sec}^{-1}$

shear rates used in figures 10 and 11. Large discrepancies were found at high shear rates (fig. 13); with decreasing shear rate the discrepancies diminished. As in the start-up data, the consistency relations for relative strain models are violated increasingly and systematically as soon as one begins to move away from the limiting region.

The computational procedures were confirmed in a variety of ways (17). The possibility that $\hat{N}_1$ calculated from $\hat{\sigma}$ may be inordinately sensitive to the precision of $\hat{\sigma}$ at long times (14) was also examined. Calculations of steady state values of $\hat{N}_1$ from $\hat{\sigma}(\dot{\gamma}, t)$ are indeed questionable for this reason. However, the discrepancies in figures 10 and 11 cannot be explained in this way. The calculated value of $\hat{N}_1(\dot{\gamma}, t)$ depends only on the behavior of $\hat{\sigma}$ for shear rates and times less then $\dot{\gamma}$ and t. In figure 11 ($\dot{\gamma} = 10.7\,\text{sec}^{-1}$) a discrepancy appears after about 0.5 seconds, and the calculated values of $\hat{N}_1$ become negative and therefore clearly unsatisfactory beyond 1.4 seconds. Figure 4 shows that, for shear rates less than $10.7\,\text{sec}^{-1}$ and times less than 1.4 seconds, $\hat{\sigma}$ is still changing rapidly and not yet approaching steady state.

The possibility of systematic experimental errors in $\hat{\sigma}(\dot{\gamma}, t)$ must also be considered. Such errors seem unlikely however, since $\hat{\sigma}(\dot{\gamma}, t)$ is found to be independent of gap angle and platen diameter (15, 17). Measurements at the same shear rate with different gap angles provide data obtained at different angular velocities and therefore different levels of whatever inertial contributions might be present. Measurements at the same shear rate with different platen diameters provide data obtained with different free surface/volume ratios and also at different magnitudes of torque and axial force. Although not impossible it would seem strange to find such potential sources of systematic error as inhomogeneous shearing, secondary flows and free surface shape disturbances to be independent of these variables.

We therefore conclude that relative strain models are inconsistent with the transient behavior of these polymer solutions. Qualitively, such models appear unable to accommodate shear stress overshoot peaks which grow rapidly with shear rate without requiring unrealistic behavior (such as negative values) in the first normal stress difference.

6. Examination of other models

We have not attempted to fit the *Carreau* model B with these data. As presented that model appears to place undue restrictions on the form of the relaxation spectrum, and we have not tried to generalize the ideas behind it to allow any $H(\tau)$ to be used. On the other hand, start-up and relaxation data from similar polystyrene solutions have been fitted fairly well by that model (10).

The structural model of *Marrucci* et al. is cast in terms of an arbitrary relaxation spectrum. With $H(\tau)$ given, the behavior of $\sigma(\dot{\gamma})$ and $N_1(\dot{\gamma})$ is governed by a single adjustable parameter a. *Marrucci* was indeed able to fit data on low density polyethylene melts with a single value of a, and went on to show rather good agreement between prediction and experiment in several

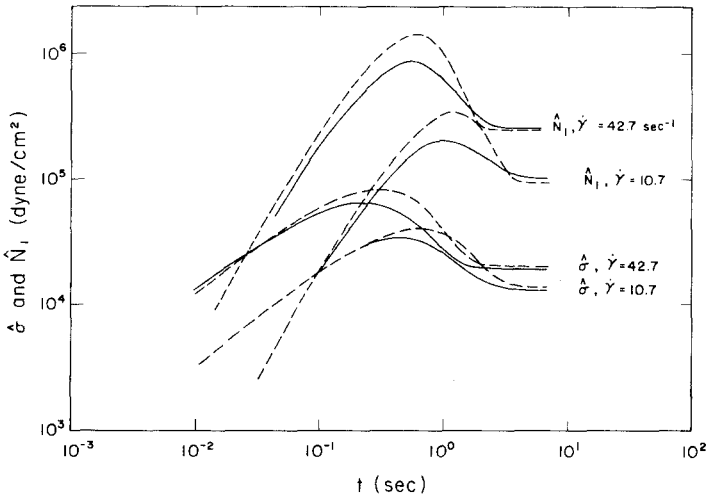

Fig. 14. Comparison of start-up curves for solution *B* with predictions based on the Marrucci model. The solid lines are experimental; the dashed lines are calculated with $a = 0.5$ for both shear rates

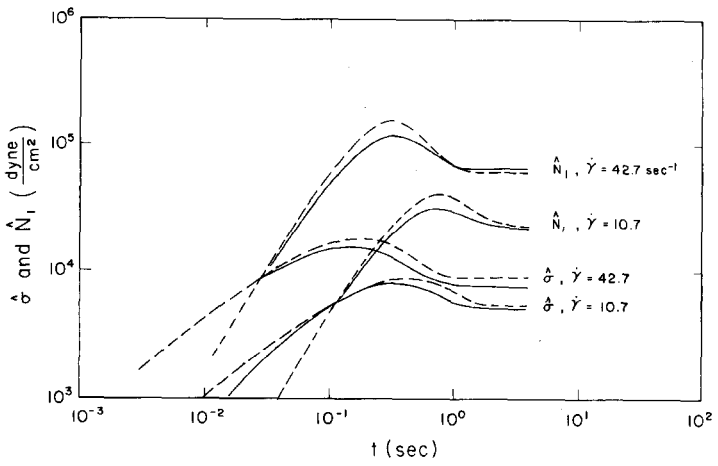

Fig. 15. Comparison of start-up curves for solution *C* with predictions based on the Marrucci model. The solid lines are experimental; the dashed lines are calculated with $a = 0.7$ for $\dot{\gamma} = 10.7\,\text{sec}^{-1}$ and $a = 0.8$ for $\dot{\gamma} = 42.7\,\text{sec}^{-1}$

types of transient flows, including start-up (22). Unfortunately, we were unable to satisfy our steady state data with a single value of a. The values required ranged from 0.2 at $\dot{\gamma} = 0.1\,\text{sec}^{-1}$ to 0.5 at $\dot{\gamma} = 100\,\text{sec}^{-1}$ for solution *B* and from 0.4 to 0.9 in the same range of shear rates for solution *C*. Nevertheless, in order to proceed with the start-up comparisons we used different values at each shear rate, choosing them to give the best compromise in fit between the steady state values of σ and N_1 at that shear rate.

Typical examples of the start-up results are given in figures 14 and 15. The time to the overshoot peak in both $\hat{\sigma}$ and $\hat{N}_1$ is predicted fairly well. The predicted peak magnitude is consistently too large in the case of $\hat{N}_1$. The major difference for $\hat{\sigma}$ is that the predicted peak width is consistently larger than observed. In the *Carreau* model B the times to peak are also fairly well predicted, but the $\hat{N}_1$ peak magnitude in that case is underestimated (see Ref. (10)). Without further comparisons it is not possible to say which model is better. We have not tested the *Marruci* model with relaxation data.

7. Conclusions

Both strain rate and relative strain models were found to be fundamentally inconsistent with the data reported here on start-up and relaxation of stress from steady state. *Marrucci*'s structural model, with adjustment of the structural parameter for each shear rate, was found to be in reasonable accord with such data. Some systematic inconsistencies are present, but they appear to be no more serious than those noted elsewhere in tests of the *Carreau* model B. Because the models must be tested on a somewhat different basis, due to the manner in which they are formulated, it is still not clear which is preferable.

Acknowledgements

We are grateful to the National Science Foundation for sponsoring this work (GK 34362 and ENG 75-15683). We are also grateful to the Plastics Institute of America for partial fellowship support to one of us (RLC) during the period this work was performed.

Summary

Stress development at the onset of steady shear flow and stress relaxation from steady state were measured in a stiffened Weissenberg Rheogoniometer over wide ranges of shear rate for three polystyrene solutions. Time dependent shear stress σ and first normal stress difference N_1 were obtained from the torque and axial thrust. From extensive auxiliary tests we believe these data to be free of spurious effects associated with instrument compliance. The solutions have zero shear viscosities of 890, 3900 and 67 000 poise. Tests for consistency with strain rate constitutive models were made using the *van Es-Christensen* relation and with relative strain models using the *Kearsley-Zapas* relations. Substantial deviations were found in both cases. The *Marrucci* model was also examined. As in the *Carreau* model B, the predicted start-up curves from the *Marrucci* model are in general qualitative accord with observations, but some systematic quantitative discrepancies remain.

Zusammenfassung

Der Spannungsaufbau beim Anfahren einer stationären Scherströmung und die Spannungsrelaxation nach dem Anhalten derselben werden in einem steifer gemachten Weissenberg-Rheogoniometer für drei Polystyrol-Lösungen über einem weiten Schergeschwindigkeitsbereich gemessen. Die zeitabhängige Schubspannung σ und die erste Normalspannungsdifferenz N_1 werden aus dem Drehmoment und der Axialverschiebung bestimmt. Aus umfangreichen Nebenuntersu-

chungen kann man schließen, daß die Ergebnisse von Verfälschungen durch instrumentelle Effekte weitgehend frei sind. Die Lösungen haben Null-Viskositäten von 890, 3900 und 67000 Poise. Für eine Untersuchung der Verträglichkeit der Daten mit Stoffgesetzen vom "strain rate"-Typ wurde die *van Es-Christensen*-Gleichung zugrundegelegt, für Stoffgesetze vom „relative strain"-Typ entsprechend die *Kearsley-Zapas*-Gleichung. In beiden Fällen wurden wesentliche Abweichungen gefunden. Ebenso wurde das Modell von *Marrucci* geprüft. Ähnlich wie beim *Carreau*-Modell B sind die Voraussagen des Anlauf-Verhaltens durch dieses Modell durchgängig in qualitativer Übereinstimmung mit den Beobachtungen, aber einige systematische quantitative Unterschiede sind auch hier vorhanden.

References

1) *Ferry, J. D.*, Viscoelastic Properties of Polymers, 2nd Ed. (New York 1970).

2) *Walters, K.*, Rheometry (London 1975).

3) *Coleman, B. D., H. Markovitz*, J. Appl. Physics **35**, 1 (1964).

4) *Graessley, W. W.*, Adv. Polymer Sci. **16**, 1 (1974).

5) *Lodge, A. S.*, Body Tensor Fields in Continuum Mechanics (New York 1974).

6) *Lodge, A. S.*, Elastic Liquids (New York 1964).

7) *Yamamoto, M.*, Trans. Soc. Rheology **15**, 331 (1971).

8) *Bernstein, B., E. A. Kearsley, L. J. Zapas*, Trans. Soc. Rheology **7**, 391 (1963).

9) *Chen, I.-J., D. C. Bogue*, Trans. Soc. Rheology **16**, 59 (1972).

10) *Carreau, P. J.*, Trans. Soc. Rheology **16**, 99 (1972).

11) *Marrucci, G., G. Titomanlio, G. C. Sarti*, Rheol. Acta **12**, 269 (1973).

12) *van Es, H. E., R. M. Christensen*, Trans. Soc. Rheology **17**, 325 (1973).

13) *Kearsley, E. A.*, Talk presented at Society of Rheology Annual Meeting, Amherst, November 1974.

14) *Kearsley, E. A., L. J. Zapas*, Trans. Soc. Rheology **20**, 623 (1976).

15) *Crawley, R. L., W. W. Graessley*, Trans. Soc. Rheology **21**, 19 (1977).

16) *Meissner, J.*, J. Appl. Polymer Sci. **16**, 2877 (1972).

17) *Crawley, R. L.*, Doctoral Thesis, Northwestern University, 1976.

18) *Macosko, C. W., W. M. Davis*, Rheol. Acta **13**, 814 (1974).

19) *Berry, G. C., C.-P. Wong*, J. Polymer Sci.: Polymer Phys. Ed. **13**, 1761 (1975).

20) *Gortemaker, F. H., M. G. Hansen, B. deCindio, H. M. Laun, H. Janeschitz-Kriegl*. Rheol. Acta **15**, 256 (1976).

21) *Chang, K. I., S. S. Yoo, J. P. Hartnett*, Trans. Soc. Rheology **19**, 155 (1975).

22) *Acierno, D., F. P. La Mantia, G. Marrucci, G. Rizzo*, and *G. Titomanlio*, J. Non-Newtonian Fluid Mech. **1**, 147 (1976).

Authors' addresses:

Prof. *W. W. Graessley*
W. S. Park
Chemical Engineering Department

R. L. Crawley
Materials Science and Engineering Department
Northwestern University
Evanston, Illinois 60201 (USA)